# RARE METALS

ORIGINAL ARTICLE

# Identification of optimal solid solution temperature for $Sm_2Co_{17}$-type permanent magnets with different Fe contents

**Shuai Wang, Hong-Sheng Chen, Yi-Kun Fang*** [iD] **, Chao Wang, Lei Wang, Ming-Gang Zhu, Wei Li*** [iD]

**Abstract** It is confirmed that the solid solution temperature range to obtain optimal magnetic properties is different for the magnets with different Fe contents, and the correlation between magnetic properties and microstructures influenced by solid solution temperature ($T_s$) has been systematically studied. The optimal solid solution temperature range is 1413–1463 K for the $Sm(Co_{bal}Fe_{0.213}Cu_{0.073}Zr0_{.024})_{7.6}$ magnet, which is higher than that of the $Sm(Co_{bal}Fe_{0.262}Cu_{0.073}Zr_{0.024})_{7.6}$ magnet (1403–1453 K), and the optimal $T_s$ range is about 50 K for both of the magnets. The solid solution temperature range shifting toward relatively high temperature is due to the increase in a phase transition temperature. The magnet solution-treated at proper temperature exhibits 1:7H single phase, and intact cell structure and high Cu concentration (23.12 at%) in the cell boundary are found after aging process, which makes the magnet shows high intrinsic coercivity ($H_{cj}$) and magnetic field at knee-point ($H_{knee}$). At a lower solid solution temperature, the 2:17H, 1:5H and Zr-rich precipitation phases appear, which affects the cell structure, density of lamellar phase and Cu concentration in the cell boundary, leading to the reduced magnetic properties. However, at a higher solid solution temperature, there exist obviously light gray and dark regions with different Sm, Cu and Fe contents in scanning electron microscopy observation, and the magnet shows low pinning field in the two regions and incomplete cell structure, resulting in an inferior $H_{cj}$ and $H_{knee}$.

S. Wang, H.-S. Chen, Y.-K. Fang*, C. Wang, L. Wang, M.-G. Zhu, W. Li*
Division of Functional Materials Research, Central Iron and Steel Research Institute, Beijing 100081, China
e-mail: ykfang@cisri.com.cn

W. Li
e-mail: weili@cisri.com.cn

## 1 Introduction

$Sm_2Co_{17}$-type sintered magnets have been widely applied in aerospace, military technology and electric cars fields due to the large magnetocrystalline anisotropies, high Curie temperature and excellent thermal stability [1–3]. It is generally known that solid solution treatment is critical for the $Sm_2Co_{17}$-type magnets to obtain high performance. Through an appropriate solid solution treatment process, a single-phase state 1:7H is formed, and it evolves into a microstructure consisting of 2:17R cells surrounded by 1:5H cell boundaries coexisting with a Zr-rich lamellar phase after aging. These typical microstructures make the magnets obtain high intrinsic coercivity ($H_{cj}$) and magnetic field at knee-point ($H_{knee}$) (a magnetic field at which the corresponding magnetization is equal to 0.9 times remanence) [4–9]. Recently, Zhang et al. [10] reported that the solid solution temperature has a far-reaching impact on the phase structure and microstructure, which determines the magnetic properties of the magnets. Xu et al. [11] also studied the correlation of microstructure and magnetic properties in $Sm_2Co_{17}$ magnets solution-treated at various temperatures. It is found that an inhomogeneity of the cellular structure is discovered in the magnets solution-treated at a higher or lower temperature. This inhomogeneity results in weak pinning field, which is accountable for the deterioration of the magnetic properties.

However, as well known, the coercivity of $Sm_2Co_{17}$-type sintered magnets mostly originates from the strength of domain wall pinning. The enrichment of Cu in the cell boundaries increases the magnetic field needed for the wall pinning [12–14]. This is the key factor for that the $Sm_2Co_{17}$-type magnets show a much higher $H_{cj}$ and $H_{knee}$. Therefore, more information about Cu distribution at the cell boundaries needs to be studied to reveal the difference of magnetic properties influenced by the solid solution temperature. Moreover, as reported in Ref. [10], there mainly exist two kinds of phase regions with obvious different contrasts in the magnet solution-treated at a higher temperature, and the corresponding microstructures should be different in the two regions, which further influences the magnetic properties of the magnet. The difference of cell structure and Cu distribution at the cell boundaries in the two regions also needs to be studied in detail.

Moreover, it was reported that Fe content of the $Sm_2Co_{17}$-type magnets also affected the morphology and elemental distribution of their microstructure [15–17]. To prepare the $Sm_2Co_{17}$-type magnets with high maximum energy product $((BH)_{max})$, more iron is added (at the expense of cobalt) to increase the saturation magnetization of the $Sm_2(Co, Fe)_{17}$ matrix phase [18, 19]. An appropriate solution process should be employed to obtain the optimal magnetic performance of the magnets with higher Fe content. However, the correlation between Fe content and solid solution temperature needs to be investigated in detail to better control the magnetic properties.

In this paper, the optimum solid solution temperature range for the magnets with various Fe contents were investigated, and the influences of solid solution temperature on the microstructures were further studied. These results provide a clue to achieve better control of the microstructures to obtain high-performance $Sm_2Co_{17}$-type sintered magnets, especially for different Fe contents.

## 2 Experimental

The magnets with nominal compositions of $Sm(Co_{bal}Fe_{0.213}Cu_{0.073}Zr_{0.024})_{7.6}$ (Magnet A, with lower Fe content) and $Sm(Co_{bal}Fe_{0.262}Cu_{0.073}Zr_{0.024})_{7.6}$ (Magnet B, with higher Fe content) were prepared by a conventional powder metallurgical technology. The ingots prepared by induction melting were crashed and jet-milled into powders with a mean particle size of 3–5 μm. Then, the powders were aligned and pressed in a magnetic field of about 2 T and followed by an isostatic pressing process. The green compacts were sintered at 1478–1488 K for 1 h and then were solid solution treated at 1363–1473 K for 4–8 h and quenched. The subsequent isothermal aging of all the magnets were at 1103–1123 K for 5–10 h, followed by
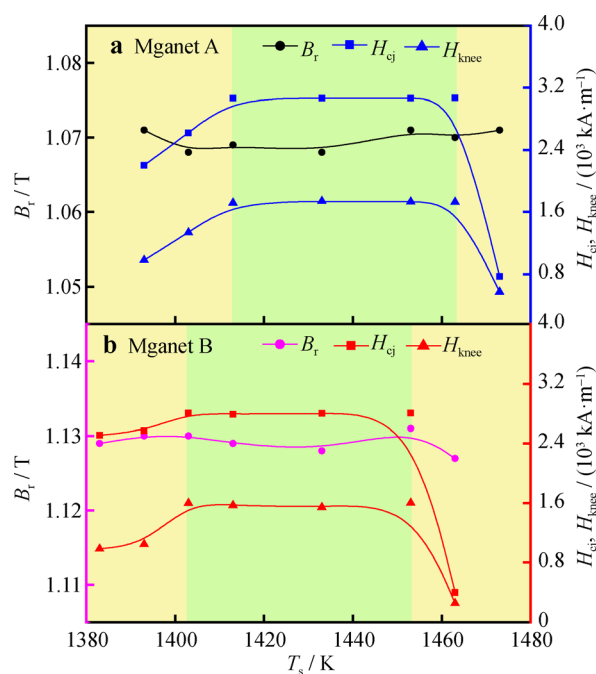


**Fig. 1** Dependence of $B_r$, $H_{cj}$ and $H_{knee}$ of magnets with different Fe contents on solid solution temperature $(T_s)$: **a** $Sm(Co_{bal}Fe_{0.213}Cu_{0.073}Zr_{0.024})_{7.6}$ (Magnet A) and **b** $Sm(Co_{bal}Fe_{0.262}Cu_{0.073}Zr_{0.024})_{7.6}$ (Magnet B)

slowly cooling to 673 K, and finally quenched to room temperature directly.

A Hirst 14 pulsed field magnetometer (PFM) with a maximum magnetic field of 10 T was used for magnetic properties measurements, and the test specimens with dimensions of $(10 \pm 0.01)$ mm in diameter and $(10 \pm 0.01)$ mm in height were cut from the aged magnets. The crystal structure of the phases was measured by a Rigaku Smartlab X-ray diffraction (XRD) with a Cu Kα radiation. Phase transitions of the as-solution-treated magnets were measured by a STA 449 F3 differential scanning calorimetry (DSC). A Phenom ProX scanning electron microscopy (SEM) equipped with an energy-dispersive spectroscopy (EDS) was used to observe the microstructure of the magnets. The focus ion beam (FIB) technique was employed for the preparation of transmission electron microscope (TEM) specimen. Detailed cell structure and elemental distribution analysis of the aged magnets were carried out by a FEI Tecnai G2 F20 TEM equipped with EDS.

## 3 Results and discussion

### 3.1 Magnetic properties and optimal solid solution temperature range of Magnets A and B

Figure 1 shows the dependence of typical magnetic properties, remanence $(B_r)$, $H_{cj}$ and $H_{knee}$ on the solid solution
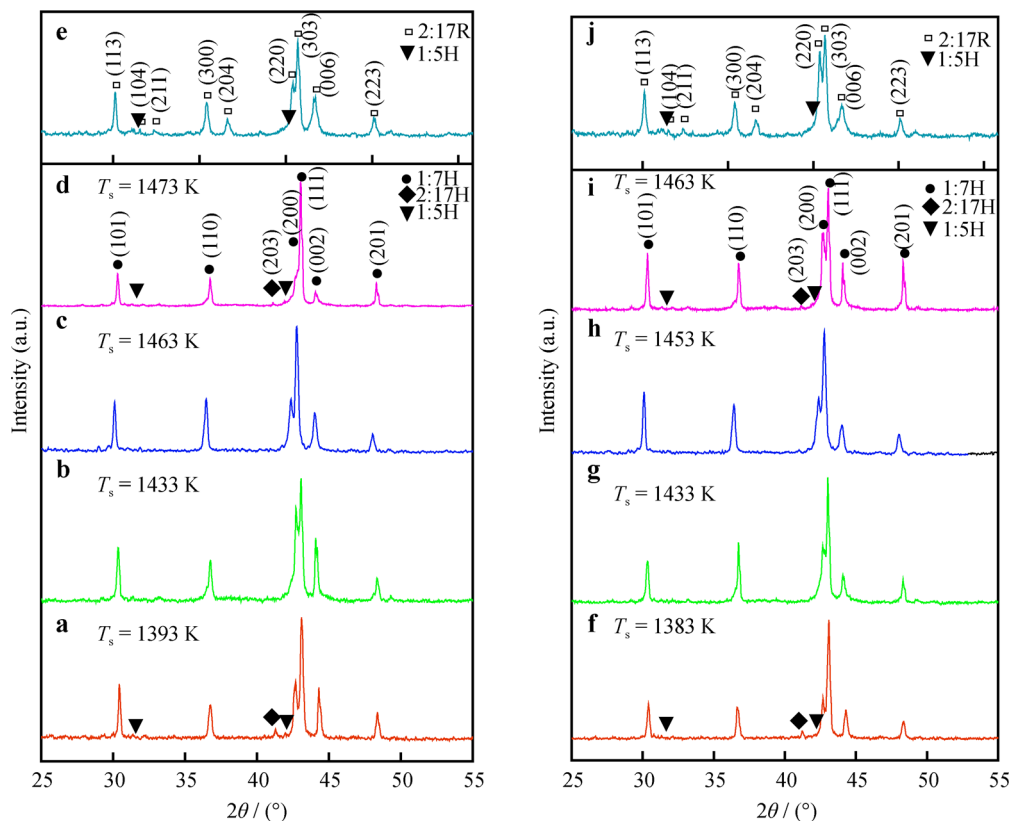
**Fig. 2** Powder XRD patterns of as-solution-treated magnets with various solution-treated temperatures ($T_s$): Magnet A, **a** $T_s$ = 1393 K, **b** $T_s$ = 1433 K, **c** $T_s$ = 1463 K, and **d** $T_s$ = 1473 K; Magnet B, **f** $T_s$ = 1383 K, **g** $T_s$ = 1433 K, **h** $T_s$ = 1453 K and **i** $T_s$ = 1463 K; powder XRD patterns of aged **e** Magnet A and **j** Magnet B

temperature ($T_s$) for Magnets A and B. As shown in Fig. 1a, b, $B_r$ is almost constant with $T_s$ increasing for the two types of magnets. For Magnet A, $H_{cj}$ and $H_{knee}$ increase from 2196.96 kA·m$^{-1}$ and 971.12 kA·m$^{-1}$, to 3048.68 kA·m$^{-1}$ and 1711.4 kA·m$^{-1}$, respectively, with $T_s$ increasing from 1393 to 1413 K, and then, they remain constant with $T_s$ further increasing to 1463 K, after that $H_{cj}$ and $H_{knee}$ drop sharply to 772.12 kA·m$^{-1}$ and 573.12 kA·m$^{-1}$ with $T_s$ further increasing up to 1473 K, as shown in Fig. 1a. While, for Magnet B, $H_{cj}$ and $H_{knee}$ increase from 2499.44 kA m$^{-1}$ and 979.08 kA m$^{-1}$, to 2793.96 kA m$^{-1}$ and 1592 kA m$^{-1}$, respectively, with $T_s$ increasing from 1383 to 1403 K, and then, they keep constant as $T_s$ continues to rise, and when $T_s$ is higher than 1453 K, $H_{cj}$ and $H_{knee}$ begin to drop sharply, as shown in Fig. 1b. It is found that 1413–1463 K is the optimum $T_s$ range for Magnet A to obtain relatively high $H_{cj}$ and $H_{knee}$, while it is 1403–1453 K for Magnet B. And the temperature range of optimal $T_s$ for Magnet B shifts to relatively low temperature compared with that of Magnet A. More impressively, the optimal $T_s$ range for magnets is both about 50 K though Fe content is different.
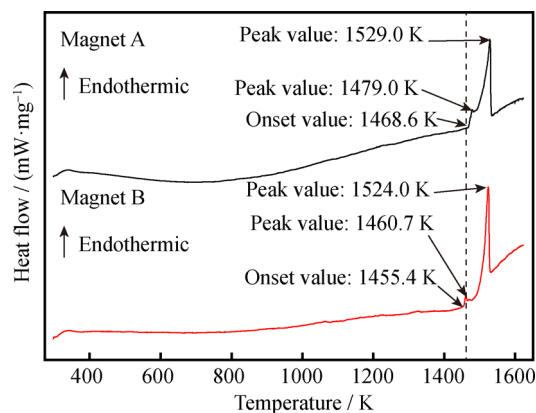


**Fig. 3** DSC curves of as-solution-treated Magnets A and B

To reveal the difference of the magnetic properties of the magnets, the phase constitution should be checked first. The powders XRD patterns of the as-solution-treated and aged Magnets A and B are shown in Fig. 2. As a whole, the 1:7H phase with a TbCu$_7$ structure is the main phase, which is found in all as-solution-treated magnets. As shown in Fig. 2b, c, g, h, the as-solution-treated Magnets A

and B with proper $T_s$ exhibit single phase structure with 1:7H phase, while 2:17H phase and 1:5H phase can be indexed for the as-solution-treated Magnets A and B with other $T_s$, as shown in Fig. 2a, d, and f, i, respectively. Except the as-solution-treated magnets, the powder XRD patterns of the aged Magnets A and B with various $T_s$ were also measured. XRD patterns are almost the same, and the aged magnets consist of 2:17R and 1:5H phases, as shown in Fig. 2e, j. Combined with the magnetic properties and XRD results, it can be found that the magnets solution-treated at proper $T_s$ obtain 1:7H single phase which is the key to obtaining optimal magnetic properties of the magnets.

To further reveal the origin of the difference of optimal $T_s$ range for Magnets A and B, their DSC curves were measured, as shown in Fig. 3. It can be found that there are two obvious endothermic peaks in both DSC curves. The relatively low peak corresponds to a phase transition process, while the high peak corresponds to the melting point of the main phase. For Magnet A, the onset and peak temperatures of phase transition are 1468.6 and 1479.0 K, respectively. And the corresponding temperatures are 1455.4 and 1460.7 K for Magnet B. It is obvious that both the onset and peak temperatures for Magnet B are lower than those of Magnet A. Based on the XRD results, the magnets solution-treated at proper $T_s$ have 1:7H single phase, while the 2:17H and 1:5H phases appear when the magnets solution-treated at a higher $T_s$. It means that some 1:7H phase decomposes into 2:17H and 1:5H phases when the $T_s$ is higher than a critical temperature. Therefore, the endothermic peaks corresponding to phase transition are found in the DSC curves. The largest optimal $T_s$ = 1463 K

is lower than the phase transition temperature of Magnet A (1468.6 K) and higher than that of Magnet B (1455.4 K). This is consistent with the results that, when solution-treated at 1463 K, good magnetic properties are obtained for Magnet A, while inferior magnetic properties for Magnet B.

### 3.2 Effects of solid solution temperature on microstructures of Magnets A and B

In order to reveal the microstructures, the magnets were characterized by SEM equipped with EDS. Typical backscattered electron (BSE) images of the as-solution-treated Magnets A and B with various $T_s$ are shown in Fig. 4. The "white" phases are $Sm_2O_3$, which have been reported in many other literatures [10, 11, 20]. As shown in Fig. 4a, there are a few precipitated phases (Region I) in the matrix phase for Magnet A solution-treated at 1393 K, and the precipitated phases (Region V) are also found in Magnet B solution-treated at 1383 K shown in Fig. 4d. The precipitation phases in Magnet A are obviously more than that in Magnet B. When $T_s$ increases to 1433 K, the precipitation phases decrease in number in Magnet A and disappear in Magnet B, as shown in Figs. 4b, e, respectively. Figure 4c, f shows that there exist two different regions: light gray region (Regions III and VI) and dark region (Regions IV and VII) in Magnet A solution-treated at 1473 K and Magnet B solution-treated at 1463 K, respectively.

Table 1 shows the compositions determined by EDS of the phases that appear in the magnets. It can be found that the matrix phase is close to the nominal composition of the
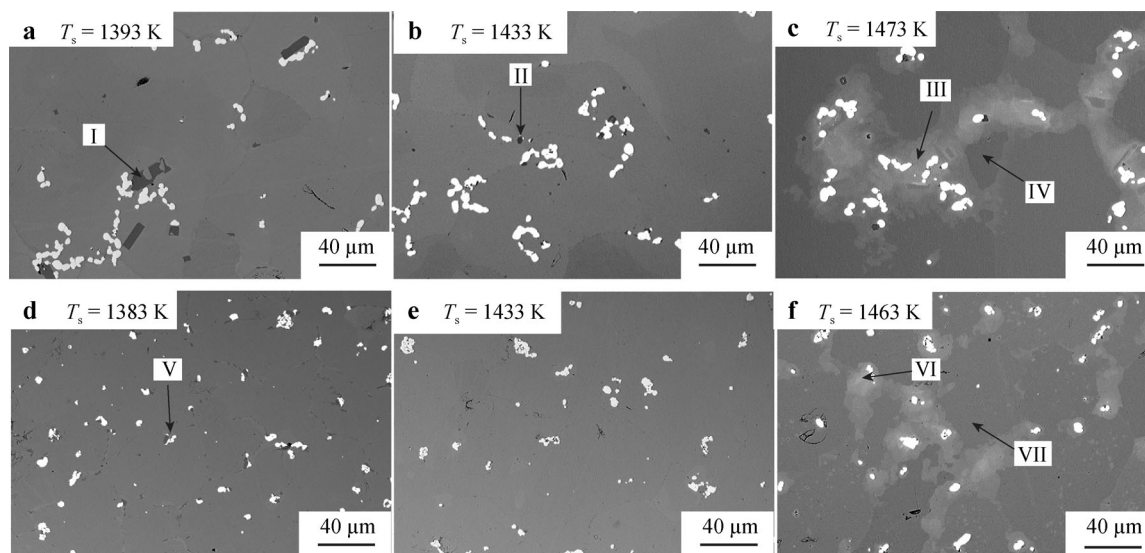


**Fig. 4** Typical BSE images of as-solution-treated magnets with different $T_s$: Magnet A, **a** $T_s$ = 1393 K, **b** $T_s$ = 1433 K, and **c** $T_s$ = 1473 K; Magnet B, **d** $T_s$ = 1383 K, **e** $T_s$ = 1433 K, and **f** $T_s$ = 1463 K

corresponding magnet. Regions I, II and V are Zr-rich phases which prefer to precipitate at a low solution temperature [10, 11], so the number of Zr-rich phases decreases significantly as the solution temperature goes up. As it is reported in Refs.[17, 21], Fe atoms have a strong preference for dumbbell Co–Co sites in 1:7H phase and promote the transformation from ordered 1:7H phase to partially ordered 2:17R phase, while the metallurgical function of Zr is to displace Fe atoms pairs by Zr-vacancy

pairs from the dumbbell sites, and thus Fe atoms must occupy the planar sites. And the magnet with higher Fe content needs more Zr-vacancy pairs to displace Fe pairs and stabilize the 1:7H phase. Therefore, Magnet B has fewer Zr-rich precipitation phases. Regions III and VI have more Sm, more Cu and less Fe, which is close to the composition of 1:5H phase, while Regions IV and VII have more Fe, less Sm and less Cu, which is close to the composition of 2:17H phase. The presence of light gray phases
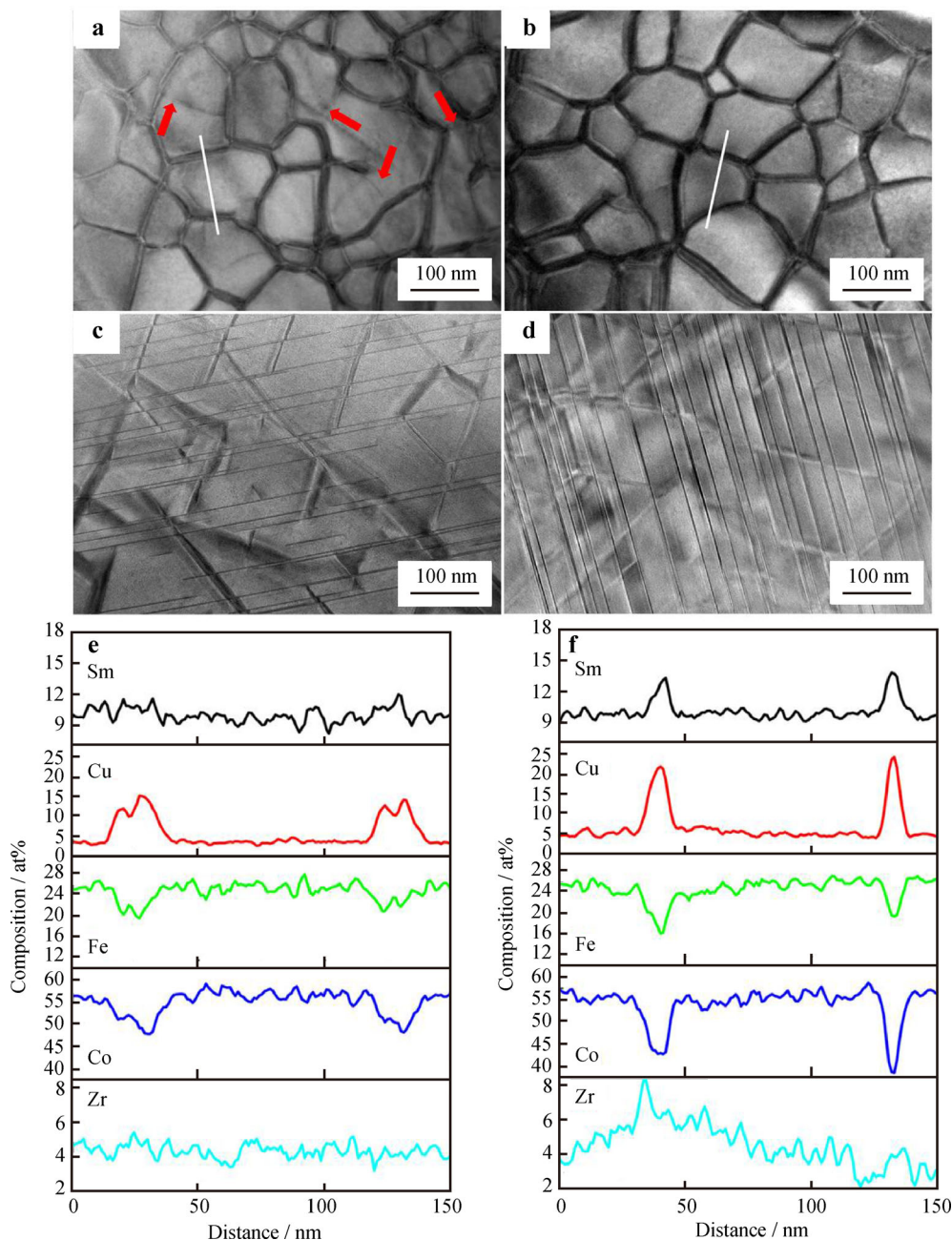


**Fig. 5** Typical TEM bright-field images of Magnet B with different $T_s$: **a** $T_s$ = 1383 K and **b** $T_s$ = 1433 K with *c*-axis perpendicular to imaging plane; **c** $T_s$ = 1383 K and **d** $T_s$ = 1433 K with *c*-axis parallel to imaging plane; composition profiles of cells and cell boundaries marked with **e** white line in **a** and **f** white line in **b**

**Table 1** Sm, Co, Fe, Cu and Zr contents of matrix and Regions I-VII shown in Fig. 4 (at%)

| Magnet | $T_s$/K | Regions | Sm | Co | Fe | Cu | Zr | Phase |
|--------|---------|---------|------|------|------|------|------|---------|
| A | 1393 | Matrix | 11.3 | 60.0 | 20.3 | 6.5 | 1.9 | 1:7H |
|   |      | I | 1.2 | 58.0 | 17.5 | 1.5 | 21.8 | Zr-rich |
|   | 1433 | Matrix | 11.2 | 58.5 | 20.3 | 7.3 | 2.6 | 1:7H |
|   |      | II | 1.2 | 57.8 | 18.0 | 1.4 | 21.5 | Zr-rich |
|   | 1473 | III | 14.9 | 53.1 | 16.1 | 14.2 | 1.7 | 1:5H |
|   |      | IV | 10.2 | 60.1 | 21.6 | 5.4 | 2.7 | 2:17H |
| B | 1383 | Matrix | 11.3 | 55.8 | 25.1 | 6.1 | 1.6 | 1:7H |
|   |      | V | 3.0 | 53.6 | 21.1 | 2.1 | 20.2 | Zr-rich |
|   | 1433 | Matrix | 10.9 | 55.8 | 24.9 | 5.9 | 2.5 | 1:7H |
|   | 1463 | VI | 15.1 | 52.8 | 17.0 | 9.7 | 5.4 | 1:5H |
|   |      | VII | 10.4 | 56.5 | 25.9 | 4.9 | 2.3 | 2:17H |

and dark phases at a higher solution temperature is consistent with the XRD results. These microstructure characteristics do not change after aging process [22, 23].

The effects of $T_s$ on the microstructures of Magnets A and B are consistent, although the optimal solution temperature range is different. To get the correlation between the magnetic properties and microstructures, the detailed nanoscale microstructure analyses on aged Magnet B were taken by a TEM. Figure 5 shows bright-field (BF) images and elemental distribution with $T_s = 1383$ and 1433 K. As shown in Fig. 5a, b, a few cell boundaries marked by red arrows are incomplete in the magnet with $T_s = 1383$ K, while the cell structure in the magnet solution-treated at 1433 K is intact. The average cell sizes are 96.3 and 94.6 nm for the magnets with $T_s = 1383$ and 1433 K, respectively. As well known, the cell structure is closely correlated to the phase component of as-solid solution magnets. It is revealed from the XRD results that the as-solution-treated magnet obtains 1:7H single phase when solution-treated at 1433 K. Therefore, after aging treatment, the magnet obtains complete cell structure. While 2:17H phase exists in the as-solution-treated magnet with $T_s = 1383$ K, which is not prone to form the ideal cell structure after aging [11, 13, 15], so there is incomplete cell structure in the aged magnet with $T_s = 1383$ K. As shown in Fig. 5c, d, the lamellar phases are observed clearly in the aged Magnets B with $T_s = 1383$ and 1433 K, and the lamellar phase densities are calculated to be 0.036 and 0.044 $nm^{-1}$, respectively. It is found that the density of lamellar phase of the magnet with $T_s = 1433$ K is higher than that of the magnet with $T_s = 1383$ K. It is due to the presence of Zr-rich precipitate phase in the magnet with $T_s = 1383$ K observed by SEM (Fig. 4d). As reported previously [4], Zr-rich phase may lead to the reduction of the lamellar phase. So the magnet solution-treated at 1383 K shows a relatively low density of lamellar phase.

Figure 5e, f shows elemental distribution along the cells and cell boundaries of the magnets marked by white lines in Fig. 5a, b, respectively. As a whole, TEM-EDS patterns show that both Co and Fe are lean in cell boundaries; however, Cu enriches in cell boundaries. For the cell boundaries of the magnets with $T_s = 1383$ and 1433 K, the average peak Cu concentrations are about 14.96 at% and 23.12 at%, respectively. As well known, the Zr-rich lamellar phase acts as the elemental diffusion paths during the aging process [24–26]. And the larger density of lamellar phase may promote the enrichment of Cu in the cell boundary. Therefore, the magnet ($T_s = 1433$ K) with larger density of lamellar phase has a higher average peak Cu concentration at the cell boundary. Higher Cu concentration in the cell boundary may result in an increased domain wall energy density difference between the 2:17R cell and 1:5H cell boundary phases, which makes the $Sm_2Co_{17}$-type sintered magnets present high coercivity [12–14, 27]. In the experiment, the magnet with $T_s = 1433$ K has complete cell structure and shows high Cu concentration in the cell boundary. As a result, high $H_{cj}$ and $H_{knee}$ are obtained in the magnet solution-treated at 1433 K. However, incomplete cell structure exists in the magnet with $T_s = 1383$ K, which is not beneficial for co-pinning the domain walls motion during demagnetization process, and the magnet has lower Cu concentration in the cell boundary compared to the magnet with $T_s = 1433$ K. Therefore, the magnet with $T_s = 1383$ K shows lower $H_{cj}$ and $H_{knee}$.

Larger elemental component difference between Regions VI and VII of Magnet B with $T_s = 1463$ K does not change after aging. In situ FIB technique was employed to prepare TEM specimens to reveal the microstructures in the two different regions of the aged Magnet B. As shown in Fig. 6b, c, the cell is small in the light gray region, while the cell structure is coarse and irregular, and cell boundaries are incomplete in the dark region of the aged magnet. The average cell sizes of light gray and dark regions are about 58.2 and 153.45 nm, respectively. As reported previously [18, 28–30], the magnets with higher Sm content or lower Fe content have smaller cell size, while it is contrary for the magnets with higher Fe content or lower Sm content. As shown in Fig. 4f and listed in Table 1, Sm and Fe contents of the light gray region (Region VI) are, respectively, about 15.1 at% and 17 at% for the as-solution-treated magnet with $T_s = 1463$ K, and Sm and Fe contents of about 10.4 at% and 25.9 at% are obtained at the dark region (Region VII). As a result, the large difference of Sm and Fe contents between the two regions leads to the cell size variation after aging.

Figure 6d, e shows elemental distribution of the cell and cell boundaries in the two regions of the aged magnets marked by white lines in Fig. 6b, c, respectively. In the light
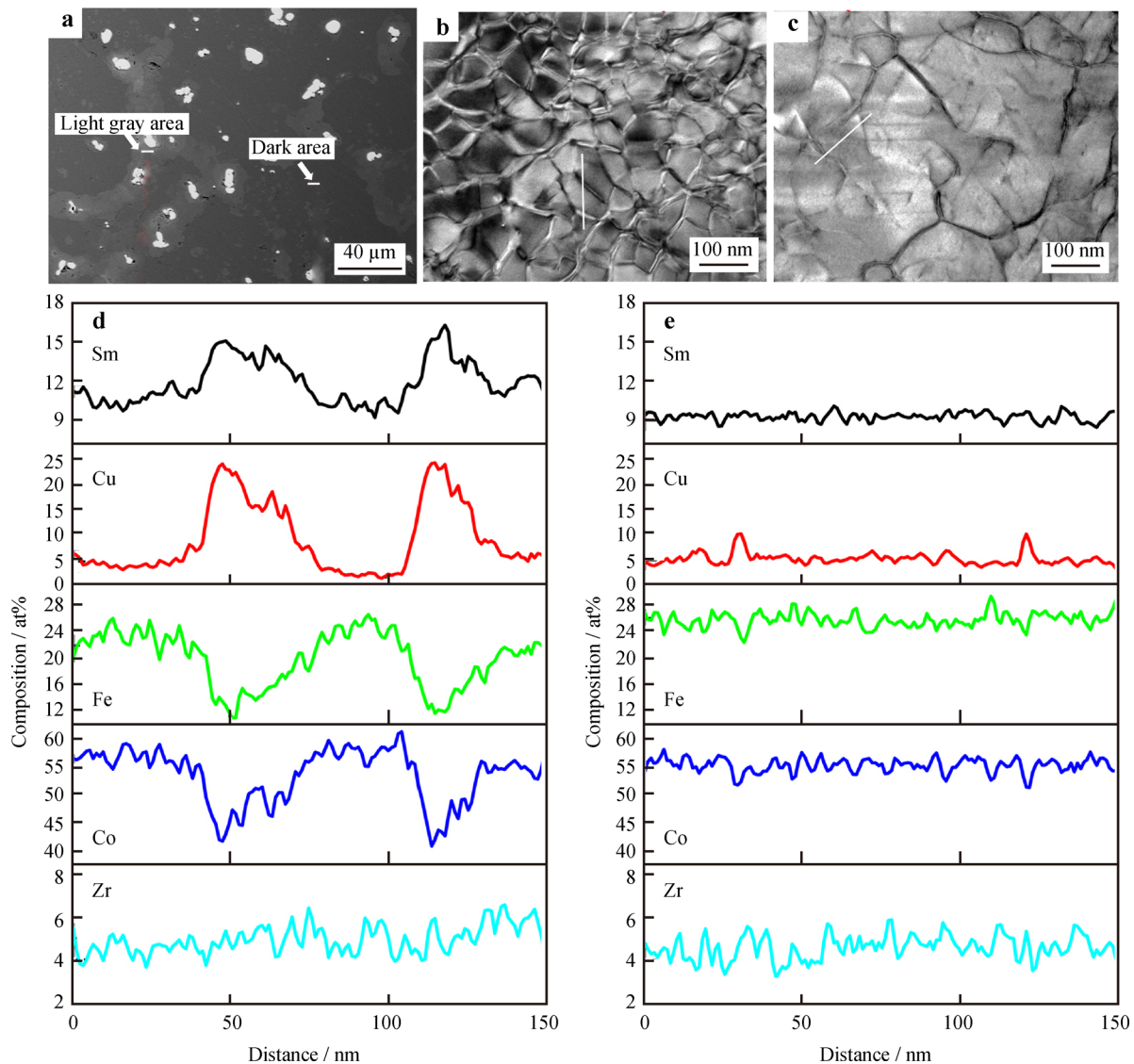
**Fig. 6** **a** Typical BSE image of aged Magnet B with $T_s$ = 1463 K (c-axis perpendicular to imaging plane); TEM bright-field images of **b** light gray area and **c** dark area in **a**: **b** light gray area and **c** dark area; composition profiles of cells and cell boundaries marked with **d** white line in **b** and **e** white line in **c**

gray region of the aged magnet, the cell boundaries have a higher average peak Cu concentration of about 24.74 at%, but the gradient of Cu concentration is very low. And for the dark region, the average peak Cu concentration is only about 10.23 at% in the cell boundaries. As the light gray region has higher Cu content than the dark region, the higher peak Cu concentration is obtained in cell boundaries in light gray region. But higher Cu content also results in a wider distribution of Cu, so the cell boundaries in the light gray region have lower Cu concentration gradient. As reported in Ref. [14], the feature of low gradient of Cu concentration may result in the lower gradient magnetocrystalline anisotropy, which reduces the pinning field of the cell boundary phase. The low pinning field in the two regions and incomplete cell

structure leads to inferior magnetic properties for the magnet with $T_s$ = 1463 K.

## 4 Conclusion

The effects of solid solution temperature on the microstructures and magnetic properties of different Fe content magnets were investigated. It is found the optimum magnetic properties can be obtained in the solid solution temperature range of 1413–1463 K for the magnet with $x$ = 0.213 (low Fe content magnet), while it is 1403–1453 K for the magnet with $x$ = 0.263 (high Fe content magnet). The 1:7H single phase is found in the magnet solution-treated at

proper temperature, while 2:17H and 1:5H phases occur at a higher or lower solution temperature. There are also more Zr-rich precipitation phases appearing in the magnet with a lower solid solution temperature. The 2:17H, 1:5H and Zr-rich precipitation phases in the as-solution-treated magnet are against the complete cell structure and high Cu concentration in the cell boundaries, leading to the reduced magnetic properties. Accordingly, the magnet solution-treated at proper temperature obtains 1:7H single phase, and after aging process, the magnet has complete cell structure and high Cu concentration (23.12 at%) in the cell boundary, showing high $H_{cj}$ and $H_{knee}$.

# References

[1] Gutfleisch O, Willard MA, Brück E, Chen CH, Sankar SG, Liu JP. Magnetic materials and devices for the 21st century: stronger, lighter, and more energy efficient. Adv Mater. 2011;23(7):821.

[2] Jiang CB, An SZ. Recent progress in high temperature permanent magnetic materials. Rare Met. 2013;32(5):431.

[3] Ojima T, Tomizawa S, Yoneyama T, Hori T. Magnetic properties of a new type of rare-earth cobalt magnets. IEEE Trans Magn. 1977;13(5):1317.

[4] Song KK, Sun W, Fang YK, Wang S, Yu NJ, Zhang ML, Zhu MG, Li W. Optimization of microstructures and magnetic properties of $Sm(Co_{bal}Fe_{0.227}Cu_{0.07}Zr_{0.023})_{7.6}$ magnets by sintering treatment. J Rare Earths. 2019;37(2):171.

[5] Fang YK, Chang HW, Guo ZH, Liu T, Li XM, Li W, Chang WC, Han BS. Magnetic microstructures of phase-separated Sm–Co 2:17-type sintered magnets. J Alloys Compd. 2008;462(1–2):376.

[6] Xiong XY, Ohkubo T, Koyama T, Ohashi K, Tawara Y, Hono K. The microstructure of sintered $Sm(Co_{0.72}Fe_{0.20}Cu_{0.055}Zr_{0.025})_{7.5}$ permanent magnet studied by atom probe. Acta Mater. 2004;52(3):737.

[7] Wang YQ, Yue M, Wu D, Zhang DT, Liu WQ, Zhang HG, Du YH. Effect of Cu redistribution in grain boundary on magnetic properties of $Sm(Co_{0.665}Fe_{0.25}Cu_{0.06}Zr_{0.025})_{7}$ permanent magnets. J Alloys Compd. 2018;741:495.

[8] Xue ZQ, Liu L, Liu Z, Li M, Lee D, Chen RJ, Guo YQ, Yan AR. Mechanism of phase transformation in 2:17 type SmCo magnets investigated by phase stabilization. Scr Mater. 2016;113:226.

[9] Yu NJ, Zhu MG, Fang YK, Song LW, Sun W, Song KK, Wang Q, Li W. The microstructure and magnetic characteristics of $Sm(Co_{bal}Fe_{0.1}Cu_{0.09}Zr_{0.03})_{7.24}$ high temperature permanent magnets. Scr Mater. 2017;132:44.

[10] Zhang TL, Song Q, Wang H, Wang JM, Liu JH, Jiang CB. Effects of solution temperature and Cu content on the properties and microstructure of 2:17-type SmCo magnets. J Alloys Compd. 2018;735:1971.

[11] Xu C, Wang H, Zhang TL, Popov A, Gopalan R, Jang CB. Correlation of microstructure and magnetic properties in $Sm(Co_{bal}Fe_{0.1}Cu_{0.1}Zr_{0.033})_{6.93}$ magnets solution-treated at different temperatures. Rare Met. 2019;38(1):20.

[12] Goll D, Stadelmaier HH, Kronmüller H. Samarium–cobalt 2:17 magnets: analysis of the coercive field of $Sm_2(CoFeCuZr)_{17}$ high-temperature permanent magnets. Scr Mater. 2010;63(2):243.

[13] Gopalan R, Hono K, Yan A, Gutfleisch O. Direct evidence for Cu concentration variation and its correlation to coercivity in $Sm(Co_{0.74}Fe_{0.1}Cu_{0.12}Zr_{0.04})_{7.4}$ ribbons. Scr Mater. 2009;60(9):764.

[14] Sepehri-Amin H, Thielsch J, Fischbacher J, Ohkubo T, Schrefl T, Gutfleisch O, Hono K. Correlation of microchemistry of cell boundary phase and interface structure to the coercivity of $Sm(Co_{0.784}Fe_{0.100}Cu_{0.088}Zr_{0.028})_{7.19}$ sintered magnets. Acta Mater. 2017;126:1.

[15] Yu NJ, Gao WY, Pan MX, Yang HF, Wu Q, Zhang PY, Ge HL. Influence mechanism of Fe content on the magnetic properties of $Sm_2Co_{17}$-type sintered magnets: microstructure and microchemistry. J Alloys Compd. 2019. https://doi.org/10.1016/j.jallcom.2019.152908.

[16] Wang YQ, Shang ZF, Yue M, Wu D, Zhang DT, Zhang HG, Liu WQ. Correlation between Fe content and z value in $Sm(Co_{bal}Fe_xCu_{0.06}Zr_{0.025})_z$ permanent magnets. J Magn Magn Mater. 2019;474:417.

[17] Zhang CY, Liu Z, Li M, Liu L, Li TY, Chen RJ, Lee D, Yan AR. The evolution of phase constitution and microstructure in iron-rich 2:17-type Sm-Co magnets with high magnetic performance. Sci Rep. 2018;8:9103.

[18] Tang W, Zhang Y, Hadjipanayis GC. Microstructure and magnetic properties of $Sm(Co_{bal}Fe_xCu_{0.128}Zr_{0.02})_{7.0}$ magnets with Fe substitution. J Magn Magn Mater. 2020;221(3):268.

[19] Horiuchi Y, Hagiwara M, Endo M, Sanada N, Sakurada S. Influence of intermediate-heat treatment on the structure and magnetic properties of iron-rich $Sm(CoFeCuZr)_Z$ sintered magnets. J Appl Phys. 2015;117:17C704.

[20] Sun W, Zhu MG, Fang YK, Liu ZY, Chen HS, Guo ZH, Li W. Magnetic properties and microstructures of high-performance $Sm_2Co_{17}$ based alloy. J Magn Magn Mater. 2015;378:214.

[21] Ray AE. Metallurgical behavior of $Sm(Co, Fe, Cu, Zr)_z$ alloys. J Appl Phys. 1984;55(6):2094.

[22] Shang ZF, Yue M, Li YQ, Zhang DT, Xie ZH, Wang YQ. The effect of multi-scale Cu distribution regulation on magnetic properties of $Sm(CoFeCuZr)_z$ magnets. J Magn Magn Mater. 2020. https://doi.org/10.1016/j.jmmm.2020.166484.

[23] Wang S, Fang YK, Song KK, Zhu XY, Wang L, Sun W, Pan W, Zhu MG, Li W. Optimization of both coercivity and knee-point magnetic field of $Sm_2Co_{17}$-type magnets via solid solution process. J Rare Earths. 2020. https://doi.org/10.1016/j.jre.2019.11.009.

[24] Rabenberg L, Mishra RK, Thomas G. Microstructures of precipitation-hardened SmCo permanent magnets. J Appl Phys. 1982;53(3):2389.

[25] Tang W, Zhang Y, Hadjipanayis GC. High-temperature magnetic properties of $Sm(Co_{bal}Fe_{0.1}Cu_{0.088}Zr_x)_{8.5}$ magnets. J Magn Magn Mater. 2000;212(1–2):138.

[26] Liafs TY, Liu Z, Feng YP, Liu L, Zhang CY, Yan GH, Feng ZX, Lee D, Yan AR. Effect of Zr on magnetic properties and electrical resistivity of $Sm(Co_{bal}Fe_{0.09}Cu_{0.09}Zr_x)_{7.68}$ magnets. J Alloys Compd. 2018;753:162.

[27] Lectard E, Allibert CH, Ballou R. Saturation magnetization and anisotropy fields in the $Sm(Co_{1-x}Cu_x)_5$ phases. J Appl Phys. 1994;75(10):6277.

[28] Liu JF, Zhang Y, Dimitrov D, Hadjipanayis GC. Microstructure and high temperature magnetic properties of $Sm(Co, Cu, Fe, Zr)_z$ (z = 6.7-9.1) permanent magnets. J Appl Phys. 1999;85(5):2800.

[29] Wang S, Fang YK, Wang C, Wang L, Zhu MG, Li W, Hadjipanayis GC. Dependence of macromagnetic properties on the microstructure in high-performance $Sm_2Co_{17}$-type permanent magnets. J Magn Magn Mater. 2020;510(5):166942.

[30] Wang C, Yu NJ, Zhu MG, Fang YK, Wang S, Li W. High temperature properties improvement and microstructure regulation of $Sm_2Co_{17}$-based permanent magnet. AIP Adv. 2019;9:125237.